J Nanopart Res (2020) 22: 248
https://doi.org/10.1007/s11051-020-04978-5

RESEARCH PAPER

^{44}Ti diffusion labelling of commercially available, engineered TiO2 and SiO2 nanoparticles

Uwe Holzwarth · **Jessica Ponti**

Received: 17 February 2020 / Accepted: 6 August 2020 / Published online: 17 August 2020

Abstract In realistic exposure scenarios, the detection and quantification of engineered nanoparticles in complex environmental or biological matrixes is a challenge since nanoparticle concentrations are frequently low and have to be discerned from a background that may contain the same elements in various chemical forms in much higher concentrations. The use of radiolabelled nanoparticles may overcome these difficulties offering high detection sensitivity without the necessity of complex sample preparation procedures. However, the labelling procedure must not alter the physicochemical and biological properties of the nanoparticles. In the present work, the radiolabelling of three different types of TiO_2 nanoparticles with primary particle sizes between 5 nm and 26 nm with commercially available ^{44}Ti has been investigated applying a simple diffusion heat treatment at 180 °C for 2.5 h on nanoparticles impregnated with a solution containing the ^{44}Ti radiolabel. The same treatment has been investigated to radiolabel amorphous SiO_2 nanoparticles with ^{44}Ti. The radiolabels are stably integrated in the nanoparticle matrix, and the release is less than 0.1% in aqueous suspension at neutral pH for at least 4 weeks. The method appears to be fast and reliable. By transmission electron microscopy, dynamic light scattering and ζ-potential measurements, only minor alterations of the nanoparticle size could be detected in the range of 1 to 2 nm.

U. Holzwarth (✉) · J. Ponti
European Commission, Joint Research Centre, Ispra, Italy
e-mail: uwe.holzwarth@ec.europa.eu

Keywords Radiolabelled nanoparticles · TiO2 nanoparticles · SiO2 nanoparticles · Diffusion labelling · Leaching · Radiolabel release · Radiolabel stability

Introduction

Investigations of the fate of nanoparticles in biological systems and environmental matrices frequently encounter the challenge to detect the applied nanoparticles on a chemically identical natural background (Gibson et al. 2011) and in very low concentrations in experimental settings mimicking realistically low exposure scenarios. It is a drawback of many investigations that they compensate for insufficient detection sensitivity by unrealistically high dosage or exposure (e.g. Krug 2014). Radiolabelled nanoparticles have been applied in in vitro (e.g. Marmorato et al. 2011; Simonelli et al. 2011; Ponti et al. 2009) and in in vivo toxicological (e.g. Schleh et al. 2013; Kreyling et al. 2017a, b, c; Xie et al. 2010; Zhang et al. 2009) and environmental studies (e.g. Kleiven et al. 2018; Chekli et al. 2016; Vitorge et al. 2014; Coutris et al. 2012; Oughton et al. 2008) where they demonstrated the advantage of very high detection sensitivity and easy quantification, usually without special specimen preparation procedures (Bello and Warheit 2017; Llop et al. 2013; Weiss and Diabate 2011). However, since the properties and behaviour of nanoparticles depend on a large variety of physicochemical parameters, utmost care is required not to change any of these during the labelling procedure. This holds especially for investigations in the framework of the risk

assessment of industrially manufactured nanoparticles in which frequently the use of nanoparticles is desired as they emerge from a large-scale industrial production process. Since the radiolabels cannot be introduced in the industrial manufacturing process, radiolabelling must be done post-manufacturing. Therefore, the effects of the radiolabelling technique on the properties of the industrial manufactured nanoparticles have to be addressed appropriately. In such tracer experiments, the distribution and quantification of the radiolabelled nanoparticles is determined on the basis of the radiation emitted by the radiolabel. This implies that the integrity of the radiolabel-nanoparticle construct has to be ensured at least over the envisaged duration of the experiments.

The situation is different for medical nanoparticles where surface functionalization is part of the strategy to target disease. In this case radiolabels, either used as tracers for diagnosis or as therapeutic agents delivering high radiation doses selectively to diseased tissues, may be loaded on the surface or in the volume of nanoparticles by chemical means during synthesis of the pharmaceutical (Kunz-Schughart et al. 2017; Dieci et al. 2017; Scheinberg et al. 2017). Nevertheless, also for medical purposes, applications were reported in which the radioactive load was created after synthesis using neutron activation of a metallic nanoparticle core (Hamoudeh et al. 2007, 2008; Buono et al. 2007; Häfeli et al. 2001).

Various purely physical radiolabelling techniques have been described that avoid chemical processing or surface functionalization, which entails the risk of altering the behaviour of the nanoparticles in the envisaged experimental environment. Probably most frequently applied are neutron activation techniques (Cotogno et al. 2016; Oughton et al. 2008; Häfeli et al. 2001). Also, techniques where activation is achieved by exposure of nanoparticles to light ion beams have been developed (Gibson et al. 2011; Holzwarth et al. 2014). However, a certain effort is required to carefully select and test the irradiation conditions, which ensure that the properties of the sensitive nanoparticles are not altered during ion bombardment (Holzwarth et al. 2012). Both techniques suffer from the drawback that access to a nuclear research reactor or a nuclear accelerator is required, respectively. In this respect diffusion labelling of nanoparticles using commercially available radionuclides may offer a faster and simpler alternative.

Analogously to the reduction of the melting temperature of nanoparticles with shrinking particle size, especially pronounced for sizes below 10 nm to 15 nm, the diffusion coefficient for self-diffusion and for foreign atoms in nanoparticles increases by even more than an order of magnitude (Jiang et al. 2004), and diffusion is facilitated by the abundant presence of defects acting as diffusion vehicles (Shibata et al. 2002). Therefore, the few diffusion steps required by an atom to penetrate a nanoparticle may occur at temperatures and within time periods which are much lower and much shorter, respectively, than for the corresponding bulk materials (Vollath 2008).

The experimental proof that the impregnation of TiO_2 nanoparticles with a solution containing ^{44}Ti followed by a temper treatment (2 h at 180 °C) leads to diffusion has been presented by Butz (2012) and Butz et al. (2011) who studied disorder in TiO_2 nanoparticles by time differential perturbed angular correlation using ^{44}Ti as a radioactive probe. ^{44}Ti decays by electron capture, and the daughter nucleus ^{44}Sc de-excites passing through an intermediate state of ^{44}Sc (with nuclear spin $I = 1$) emitting a γ-γ-cascade with energies of 78 keV and 68 keV (see Butz et al. (2011)). Since the ^{44}Sc in its intermediate state exhibits a nuclear quadrupole moment, which interacts with the local electrical field gradient on its lattice site, the nucleus undergoes a precessional motion which disturbs the angular correlation between the emission directions of the first and the second γ-photon. In several TiO_2 nanomaterials, such as ST-01 and P25 nanoparticles, Butz could identify a precession frequency, which was close to the precession frequency of the ^{44}Sc when the ^{44}Ti decays on a Ti lattice site in (monocrystalline) bulk TiO_2. This volume signal was broader than the signal known from large bulk TiO_2 which indicates contributions of decays that occurred on lattice sites with variable depth below the surface and highly variable disorder caused by distortions and defects of the crystal lattice leading to deviations from the precession frequency of the ^{44}Sc on a perfect lattice site. In all materials a second signal was detected, which can be attributed to decay sites where the electrical field gradient is modified due to the vicinity of a surface where the broken symmetry affects the electrical field gradient on the decay site of the ^{44}Ti atom (Butz 2012). Except for the smallest nanoparticles investigated, the surface signal had a much lower intensity than the volume signal, indicating that more probes decayed in the volume of the nanoparticles than close to their surface, which clearly proofs that the ^{44}Ti atoms penetrated into the nanoparticles by diffusion. The less

intense surface signal was much sharper than the volume signal. This was attributed to highly mobile H atoms terminating the surface. Their fast motion creates a much more homogeneous average field gradient on the surface decay sites, which is known in solid-state spectroscopy as motional narrowing (Butz 2012; Butz et al. 2011). Additionally, since the electrical field gradient depends of the crystal structure of the material, this method allows to distinguish contributions from the different polymorphs of the TiO_2.

Hildebrand and Franke were the first to apply this approach to produce stable ^{110m}Ag-labelled silver nanoparticles by impregnating powdered Ag nanoparticles with a [^{110m}Ag]$AgNO_3$ solution (Hildebrand and Franke 2012). Then they extended the method to label TiO_2 Aeroxide® P25 with ^{44}Ti and ^{45}Ti (Hildebrand et al. 2015). The labelling stability was assessed by determining the fraction of free ^{44}Ti radioactivity over a period of up to 28 days after diffusion labelling. During the whole observation period, the free ^{44}Ti activity was found to stay well below 0.5% for all pH conditions (ranging between pH = 2 and pH = 10), which indicates sufficiently stable radiolabelling. While the ^{45}Ti could be produced with a locally available mini-cyclotron, its physical half-life of $t_{½} = 3.08$ h is too short-lived for most applications. However, the ^{44}Ti with a physical half-life of $t_{½} \approx 60$ years (59.2 ± 0.6 years (Ahmad et al. 1998)) could not be produced with the available cyclotron and was rather expensive in commerce, which was considered a problem for a broader application.

The motivation for the present work to look again into ^{44}Ti-duffusion labelling was (i) the increasing demand for intrinsic (radio)-labelling (Jin et al. 2017; Goel et al. 2014) and (ii) the question whether the method would be equally successful with stable long-term integration of ^{44}Ti atoms in other industrially manufactured TiO_2 materials with different crystalline structures (cf. Vandebriel et al. 2018). (iii) Since neither neutron activation nor charged particle activation of Si yields adequate radiolabels for biokinetics and biodistribution studies, it was investigated whether diffusion labelling with ^{44}Ti could be applied to commercially available SiO_2 nanoparticles. Making use of the ^{18}O(p,n)^{18}F nuclear reaction, the PET (positron emission tomography) tracer ^{18}F could be produced (Pérez-Campaña et al. 2012, 2013). However, ^{18}F ($T_{½} = 110$ min) is too short-lived for biokinetics studies exceeding a few hours, and ^{18}O has a natural abundance of only 0.2% of the oxygen which limits the amount that can be produced from isotopically non-enriched SiO_2 nanomaterial as it is industrially produced.

The availability of ^{44}Ti is going to improve very likely as it is the mother radionuclide of ^{44}Sc which has been spotted as a candidate label for PET tracers and in combination with ^{43}Sc for theranostic applications in cancer treatment. Making available ^{44}Ti/^{44}Sc generators to hospitals would allow them to apply such theranostic systems without the need for an own cyclotron (Radchenko et al. 2017; Pruszyński et al. 2010). From this development one may expect an increased availability of ^{44}Ti at lower cost in near future.

Future practical applications of ^{44}Ti-labelled TiO_2 nanoparticles might include studies on the fate of TiO_2 nanoparticles in simulated environments, where (due to the inertness of TiO_2) accumulation effects in water, groundwater, soil and waste water treatment residues may be expected. For such experiments the much longer half-life of ^{44}Ti would be an asset and outweigh the rather strict precautions for laboratory space, radioactive waste management and radiation protection imposed by handling of long-lived radionuclides. In any case stable radiolabelling is a prerequisite for such studies.

Since it is not feasible to predict a priori all possible experimental conditions in which ^{44}Ti-labelled nanoparticles might be applied in the future, the present work focuses on the stability of the radiolabels in pH neutral aqueous stock solutions of the TiO_2 nanomaterials and the amorphous SiO_2 nanomaterial compiled in Table 1.

Materials and methods

Materials

^{44}Ti was purchased as non-carrier added ^{44}Ti dissolved in 4 M HCl from Los Alamos National Laboratory (USA) in 2004 with a radionuclidic purity > 99.8%. From this batch 300 kBq in a volume of 640 μL were still available for the experiments.

Four types of nanoparticles were selected for the labelling experiments. The main criteria were a similar size of the primary particles, while the crystal structure, i.e. the polymorphs of TiO_2, should vary. Previous experience with radiolabelling of these materials with different methods and continuous requests for radiolabelling were an asset. These selection criteria

Table 1 Synopsis of the nanomaterials selected for the present radiolabelling study

Material and main selection criteria	TiO_2 ST-01 Ishihara, Osaka (Japan)	TiO_2 Aeroxide® P25 (*) Evonik (Germany)	TiO_2 NM01004a (= NM104) UV Titan M212 (Sachtleben)	NM200
Material Source	Courtesy of W.G. Kreyling (Helmholtz Zentrum, Munich, Germany)	Courtesy of K. Franke and H. Hildebrand (Helmholtz Zentrum, Dresden, Germany)	JRC Repository of Representative Manufactured Nanomaterials (Totaro et al. 2016)	
Primary particle size	7 nm (XRD line width, Scherrer equation) (Inagaki et al. 2009, Holzwarth et al. 2012)	Mean diameter 21–23 nm for anatase; 20–60 nm for rutile (Rasmussen et al. 2014)	20–27 nm (XRD line width, Scherrer equation), elongated, rounded primary particles (Rasmussen et al. 2014)	Primary particles of about 20 nm (TEM, Rasmussen et al. 2013)
Agglomeration	50–60 nm (Horikoshi et al. 2011), chain-like aggregates of about 75 nm (Kreyling et al. 2017a)	DLS: agglomerates typically 125 to 156 nm (Rasmussen et al. 2014)	DLS: agglomerates, typically 125 to 130 nm (Rasmussen et al. 2014)	Polydisperse; in Milli-Q water two DLS maxima at 51 nm (9%) and 290 nm (81%), PDI = 0.53 (Holzwarth et al. 2014)
Crystal structure	Pure anatase (Inagaki et al. 2009, Holzwarth et al. 2012)	81 to 88% anatase and 12 to 19 ≈ 14% rutile (Rasmussen et al. 2014)	Rutile (stabilized by Al_2O_3 doping (Gesenhues 1997); 32,200 ppm Al by EDS (Rasmussen et al. 2014)	Precipitated synthetic amorphous SiO_2
Specific surface area	316 m^2/g (Horikoshi et al. 2011)	35–65 m^2/g (Hildebrand et al. 2015)	57 m^2/g (Rasmussen et al. 2014)	190 m^2/g (Rasmussen et al. 2013)
Experience with radiolabelling and applications	^{48}V radiolabelling by proton bombardment; successfully applied in in vivo biokinetics and biodistribution studies (Kreyling et al. 2017a, b, c)	Radiolabelling via in diffusion of ^{44}Ti and ^{45}Ti; ^{7}Be and ^{48}V radiolabelling by proton bombardment (Hildebrand et al. 2015)	^{48}V radiolabelling by bombardment with protons for in vitro experiments under UV-light exposure (unpublished)	^{7}Be-recoil radiolabelling by proton bombardment when mixed with LiCl (Holzwarth et al. 2014); interest in quantification of intestinal uptake (EFSA 2018)

The main selection criteria were approximately the same primary particle size while varying the crystal structure and demand for radiolabelling of the materials. (*) corresponds to NM105 (OECD (2015))

and the most relevant properties of the nanomaterials are compiled in Table 1.

γ-Ray spectrometry

The ^{44}Ti was quantified using its γ-ray emissions at 67.9 keV and 78.3 keV (Chu et al. 1999). The γ-ray spectra were evaluated using the software package GENIE 2000 (Canberra Inc., USA). Due to the long physical half-life of ^{44}Ti, no decay corrections was required in the present experiments.

The absolute activities of stock solutions and all specimens were determined by γ-ray spectrometry using high purity germanium (HPGe) detectors from Canberra (USA) and EG&G Ortec (USA). In order to reduce the background of environmental radioactivity, the spectrometers were shielded with lead. Additionally, the recorded spectra were corrected using background spectra that were recorded for each HPGe detector. The spectrometers were calibrated in energy and efficiency with certified standard calibration sources which exhibited an activity uncertainty of 1–1.5%.

Depending on the shape (15-mL Falcon tubes with and without centrifugal filter; 50-mL Falcon tubes with and without centrifugal filter; glass vials with flat bottom) and activity of the specimens (low activity filtrates, high activity on centrifugal filters), different measurement geometries were used. Since no calibration sources

were available for these specific geometries, the geometry effect was checked with a drop of ^{44}Ti solution (4.8 kBq) which was first measured in a glass vial and then with 1 mL of water added, transferred in a 15-mL Falcon vial, and from there in a 50-mL Falcon vial topped up to a volume of 4 mL with water. All results coincided within 10%, which was smaller than the activity uncertainty of 15% given by GENIE 2000.

Small ^{44}Ti activities in most filtrates of 1 mL from leaching studies had to be measured with a data acquisition time of 24 h in order to quantify ^{44}Ti activities as low as 0.1 Bq.

Diffusion labelling of TiO_2 nanoparticles

Nanoparticles were weighed and impregnated with the ^{44}Ti dissolved in 4 M HCl in a 20-mL glass vial. For 10 mg of nanoparticles, typically 150 μL of the ^{44}Ti solution were used. The vial with the slurry was then transferred into a preheated vacuum furnace, and the impregnated nanoparticles were subjected to a temperature of 180 °C for 2.5 h. Initially, the pressure in the vacuum furnace was adjusted to 850 mbar in order to facilitate drying and as a precaution against hypothetical escape of radioactivity during a thermal treatment. Then the valve connecting the furnace with the vacuum pump was closed, and the degradation of the vacuum due to the evaporation of the water was accepted. After 2.5 h the heating was switched off, and the vial was allowed to cool down to room temperature.

After this treatment the dried nanoparticle powder was recovered from the diffusion treatment vial. For this purpose 4 mL of 10 mM HCl was added to the vial, and the vial was subjected to a direct ultrasound treatment for 3 min to detach nanoparticles from the glass ware. During the sonification twice 3 mL of Milli-Q water (filtered using a 0.22-μm membrane filter) was added.

The suspension (10 mL) was then transferred into a 50-mL Falcon vial equipped with a 10 kDa centrifugal filter for washing and determination of the labelling yield. The washing procedure was adjusted and improved during the experiments. Washing was performed at least once using 10-mM HCl in order to facilitate removing weakly bound radiolabels from the nanoparticle surface and then using Milli-Q water until the activity measured in the liquid phase was below 1 Bq of ^{44}Ti. Such a low residual-free activity was required in order to keep the background sufficiently low for the subsequent leaching studies. Centrifugation was carried out at a relative centrifugal force of 2700 *g* for 45 min at 4 °C. After the first centrifugation of the 10-mL suspension recovered from the processing vial, the lost liquid was replaced by 4 mL (10 mM HCl or Milli-Q water) in each further washing step.

After the last washing step, the nanoparticles were recovered from the filter with a pipette repeatedly flushing the filter with 200 μL high purity Milli-Q water and transferring the nanoparticles for storage in a 50-mL Falcon vial. Based on the experience gained in the first experiment (see Table 1), this procedure was repeated up to 25 times until the liquid transferred into the Falcon vial appeared clear and no longer white and milky. After recovery, the residual activity on the filter A_{filter} was determined, and the corresponding masses of the nanoparticles lost on the filter and those recovered were calculated. The recovered nanoparticle suspensions were diluted using high purity Milli-Q water to a total volume of 10 mL or 20 mL in order to establish a concentration of around 0.5 mg/mL. No dispersants or stabilizers were added.

The suspension was then homogenized by a direct ultrasound treatment using a digital sonifier (Branson Ultrasonics Corporation, Model 450) equipped with a tapered microtip directly immersed into the suspension. The power amplitude of the device was set to 50%, and ultrasound was applied for 45 min. The power input into the suspension was calibrated (Taurozzi et al. 2011) by measuring the temperature increase during 300 s in water under identical geometrical conditions (vial type, filling and immersion of microtip), which led to a value of 0.2 W/mL which translates into a total applied energy of 540 J/mL. In order to avoid an excessive temperature increase of the nanoparticle suspension, during sonication the Falcon vial was itself immersed in a 450-mL isopropanol bath with an initial temperature of − 18 °C in a 500-mL beaker. The suspension was still below room temperature after sonication. For each sonication treatment, a cold isopropanol bath directly from the freezer was used.

Determination of nanoparticle losses during processing, labelling yield and fraction of unbound, free ^{44}Ti

The mass of nanoparticles loaded into the glass vial and subjected to the diffusion labelling was initially determined by weighing as m_0. The nanoparticles were impregnated with typically about 150 μL of $^{44}TiCl_4$ solution per 10 mg of nanoparticles. The applied ^{44}Ti

activity was determined as A_0. The emptied glass vial exhibited a ^{44}Ti activity of A_{vial}, which is related with a mass m_{vial} of nanoparticles that were lost for further processing. This mass can be calculated as

$$m_{vial} = m_0 \frac{A_{vial}}{A_0} \quad (1)$$

and the nanoparticle mass which is then subjected to a washing treatment can be calculated as

$$m_{wash} = m_0 - m_{vial} = m_0 \left(1 - \frac{A_{vial}}{A_0}\right) \quad (2)$$

After the last washing by centrifugal filtration was completed, the nanoparticles were recovered using repeatedly small volumes of Milli-Q water (200 μL) to wash the filter and to transfer the liquid in a 50-mL Falcon vial for storage. This recovery of washed nanoparticles is never complete. After the recovery of the nanoparticles, the filter exhibits a residual ^{44}Ti activity of A_{filter} from which the mass of nanoparticles that were lost on the centrifugal filter can be calculated. The mass of the nanoparticles m_{wash} that were washed was initially associated with the ^{44}Ti activity $A_0 - A_{vial}$. However, after washing, the same mass is associated with an activity which is reduced by the sum of the ^{44}Ti that was washed out in each of the washing steps. Therefore, assuming that nanoparticles cannot cross the centrifugal filter,

$$m_{filter} = m_{wash} \frac{A_{filter}}{A_0 - A_{vial} - \sum_i A_{step,i}} \quad (3)$$

holds, which allows then to calculate the mass of the nanoparticles recovered in the stock suspension as

$$m_{rec} = m_{wash} - m_{filter} = m_{wash} \left(1 - \frac{A_{filter}}{A_0 - A_{vial} - \sum_i A_{step,i}}\right) \quad (4a)$$

$$m_{rec} = m_0 \left(1 - \frac{A_{vial}}{A_0}\right) \left(1 - \frac{A_{filter}}{A_0 - A_{vial} - \sum_i A_{step,i}}\right) \quad (4b)$$

This value was then used to calculate the mass concentration of the nanoparticles in the stock solution and the activity concentration of the nanoparticles.

The labelling yield is determined as

$$Y = \frac{A_0 - A_{vial} - \sum_i A_{step,i}}{A_0 - A_{vial}} \quad (5)$$

where we have to consider the activity of ^{44}Ti that had been washed out in all executed washing steps (i = 1 …. up to 20). The activity $A_0 - A_{vial}$ takes into account only the nanoparticles that were subjected to the washing since the activity of those retained in the diffusion processing vial contains both the stably labelled ^{44}Ti atoms as well as those loosely bound on the surface.

For the leaching experiments, a certain volume of suspension has been subjected to filtration, and the fraction of free ^{44}Ti, f_{free}, has been determined from the activity measured on the filter after complete filtration, A_{NP}, which was ascribed to the nanoparticles, and the activity of the liquid filtrate, A_{liquid}, according to

$$f_{free} = \frac{A_{liquid}}{A_{NP} + A_{liquid}} \approx \frac{A_{liquid}}{A_{NP}} \quad (6)$$

where $A_{NP} >> A_{liquid}$ is the normal case yielding values of f_{free} below 10^{-3}.

Nanoparticle characterization

Hydrodynamic size distributions and ζ-potentials of the ^{44}Ti diffusion-labelled nanoparticles were determined in aqueous suspensions using Milli-Q water (filtered using a 0.22-μm membrane filter) after homogenization with ultrasound. No dispersants or stabilizers were added. The concentration was adjusted to 0.1 mg/mL by adding the appropriate quantity of Milli-Q water. The analysis was performed by dynamic light scattering (DLS) using a Zetasizer Nano ZS (Malvern Instruments Ltd., Malvern, UK). The specimens were equilibrated for 180 s at 25 °C, and the DLS measurements were performed triplicate, and the results averaged using the software provided with the instrument.

The same instrument was used to determine the ζ-potential through the electrophoretic mobility of the nanoparticles making use of the Henry equation and the Smoluchowski approximation. The specimens were equilibrated for 600 s at 25 °C, and 25 runs were performed using the automatic attenuation and voltage selection of the instrument. The results were averaged using the software provided with the instrument. In order to get reproducible and comparable measurements for the TiO_2 nanomaterials, the pH was adjusted to pH ≈

3 by addition of 10 mM HCl. The measurements on the NM200 SiO_2 nanoparticles could reproducibly be performed at the neutral pH of the stock suspension. In this case 10 mM NaCl solution (filtered using a 0.22-μm membrane filter) was added in order to increase the electrical conductivity of the suspension to about 1 $mS \cdot cm^{-1}$.

For the preparation of TEM specimens, carbon-coated TEM grids (carbon type-B, 200 mesh copper grids, supplied by TED Pella Inc., Redding, CA, USA) were stained with Alcian blue (2 mg/mL) immediately before the nanoparticles were applied in order to increase the hydrophilicity of the grids and to reduce the tendency of the nanoparticles to cluster on the grid when drying the suspension. For this purpose the grid was placed face down for 10 min on a drop of Alcian blue solution. Excessive staining was removed by passing the grid sequentially over 5 drops of Milli-Q water. Excessive water was removed by blotting the edge of the grid on a strip of filter paper. Nanoparticles were applied by placing the conditioned coated side of the grid on a drop of nanoparticle suspension. TEM investigations were performed on a JEOL 2100 microscope operated at an acceleration voltage of 200 kV. Digital images were analysed with the software Gatan Digital Micrograph supplied by JEOL with the TEM instrumentation. However, due to the sometimes very small and highly agglomerated nanoparticles, the software frequently could not unambiguously delineate the nanoparticles. Therefore, the minimum and maximum Feret diameter was determined manually on at least 300 nanoparticles.

Leaching experiments

Leaching experiments were performed with the aim to determine the increase of free ^{44}Ti in the stock suspension. For this purpose at a given time point, the stock suspension was vortexed for 1 min, and a volume of 1 mL was transferred in a 30 kDa centrifugal filter in a 15-mL Falcon vial. Centrifugation was done with a relative centrifugal force of 3461 *g* for 20 min. Then the ^{44}Ti radioactivity of the vial has been determined without the filter and the liquid centred on the detector cap. The usually low activities (close to the detection limit) frequently required measuring times of 24 h. Then the measurement was repeated with the filter in the vial and the filter centred on the detector cap. The ratio of free ^{44}Ti was determined as the ratio of the activities determined without and with the centrifugal filter according to Eq. (6).

Results

^{44}Ti diffusion labelling yields

The parameters and the results of the ^{44}Ti diffusion labelling experiments are compiled in Table 2. The labelling of the ST-01 material has been repeated three times. In the first experiment, the washing was done in only two steps. Since the nanoparticles were recovered from the processing glass vial with 4 mL of 10 mM HCl, the first washing step can always be considered washing with HCl. In the first experiment, washing was finished after the second step with Milli-Q water leaving a fraction of free ^{44}Ti of $4.4 \cdot 10^{-4}$. In all further experiments, the washing was carried on until the ^{44}Ti activity determined in the filtrate was well below 1 Bq, in order to start the leaching experiments on a lower background of free ^{44}Ti in the stock suspension. For the materials P25, the first washing step yielded nearly 0.5 kBq of free ^{44}Ti. Therefore, it was decided to execute the next washing steps with 10 mM HCl until a level of free activity could be reached similar to the value determined after the second washing of the ST-01 material. It turned out that the washing of P25 and of NM01004a required more intense washing than the ST-01 material. For the ST-01 material, at maximum ≈ 0.5% of the ^{44}Ti could be washed out (sum over all washing steps) which is equivalent with a labelling yield of ≥ 99.5%. For the P25 and the NM01004a material more than 1% and more than 2.5% of the ^{44}Ti was washed out, respectively, which corresponds to labelling yields of about 98.8% and 97.5% for P25 and NM01004a, respectively.

In the amorphous SiO_2 matrix, only 38.9% of the applied ^{44}Ti activity was stably integrated after applying the same thermal diffusion treatment as for the TiO_2 material. Due to the time-consuming centrifugal filtration, the washing could not be accomplished in one workday. After the last washing step on the first day still using 10 mM HCl, the missing liquid on the centrifugal filter was replaced by Milli-Q water in order to avoid drying of the nanoparticles on the filter overnight. The first washing steps on day two using Mill-Q water yielded again higher released ^{44}Ti activities as at the end of day one (labelled (**) in Table 2). A total of 20 washing steps were required to finally reach an activity of less than 1 Bq of ^{44}Ti in the filtrate. This corresponded to a fraction of free ^{44}Ti of about 10^{-4}.

In Table 2 the mass of the nanoparticles m_0 is given, which is subjected to the diffusion treatment and the

Table 2 Synopsis of ^{44}Ti diffusion labelling experiments

	ST-01 Exp. I	ST-01 Exp. II	ST-01 Exp. III	P25	NM01004a	NM200
m_0	5.0 mg	10.8 mg	10.6 mg	6.5 mg	6.0 mg	5.9 mg
A_0	46,000 Bq	64,000 Bq	65,000 Bq	52,000 Bq	38,000 Bq	26,000 Bq
A_{vial}	375 Bq	1200 Bq	1700 Bq	2900 Bq	3400 Bq	370 Bq
$m_{NP,vial}$	0.04 mg	0.20 mg	0.28 mg	0.36 mg	0.54 mg	0.08 mg
m_{wash}	4.96 mg	10.6 mg	10.32 mg	6.14 mg	5.46 mg	5.82 mg
$A_{step,1}$	210 Bq(*)	20 Bq(*)	220 Bq(*)	460 Bq(*)	580 Bq(*)	5600 Bq(*)
$A_{step,2}$	20 Bq	9 Bq	3 Bq	50 Bq(*)	140 Bq(*)	240 Bq(*)
$A_{step,3}$		1 Bq	1 Bq	19 Bq(*)	60 Bq(*)	1800 Bq(*)
$A_{step,4}$		0.6 (<1) Bq	1 Bq	14 Bq(*)	50 Bq(*)	2400 Bq(*)
$A_{step,5}$			0.5 (<1) Bq	14 Bq	40 Bq	1500 Bq(*)
$A_{step,6}$				4 Bq	3 Bq	580 Bq(*)
$A_{step,7}$				1 Bq	0.7 (< 1) Bq	200 Bq(*)
$A_{step,8}$				1 Bq		140 Bq(*)
$A_{step,9}$				5 Bq		130 Bq(*)
$A_{step,10}$				1 Bq		430(**) Bq
$A_{step,11}$				1 Bq		950 Bq
$A_{step,12}$				0.5 (<1) Bq		730 Bq
$A_{step,13}$						410 Bq
$A_{step,14}$						280 Bq
$A_{step,15}$						210 Bq
$A_{step,16}$						50 Bq
$A_{step,17}$						7 Bq
$A_{step,18}$						1 Bq
$A_{step,19}$						1 Bq
$A_{step,20}$						0.9 (<1) Bq
$\sum_i A_{step,\,i}$	230 Bq	30 Bq	235 Bq	570 Bq	873 Bq	15,660 Bq
Yield	99.50%	99.95%	99.63%	98.84%	97,48%	38.86%
Free ^{44}Ti	$\approx 4.4{\cdot}10^{-4}$	$\approx 1{\cdot}10^{-5}$	$\approx 8{\cdot}10^{-6}$	$\approx 1{\cdot}10^{-5}$	$\approx 2{\cdot}10^{-5}$	$\approx 9{\cdot}10^{-5}$
A_{filter}	10,900 Bq	1400 Bq	1000 Bq	4200 Bq	1400 Bq	550 Bq
m_{filter}	1.20 mg	0.24 mg	0.17 mg	0.56 mg	0.25 mg	0.33 mg
A_{rec}	34,500 Bq	61,400 Bq	62,100 Bq	44,300 Bq	32,300 Bq	9400 Bq
m_{rec}	3.77 mg	10.36 mg	10.16 mg	5.61 mg	5.23 mg	5.50 mg
Act. Conc.	9200 Bq/mg	5900 Bq/mg	6100 Bq/mg	7900 Bq/mg	6200 Bq/mg	1700 Bq/mg
Mass conc.	0.38 mg/mL	0.52 mg/mL	0.51 mg/mL	0.56 mg/mL	0.52 mg/mL	0.55 mg/mL
	3500 Bq/mL	3100 Bq/mL	3100 Bq/mL	4400 Bq/mL	3200 Bq/mL	940 Bq/mL

Compiled are the used ^{44}Ti activity A_0 and the nanoparticle mass m_0 subjected to the diffusion labelling treatment, the measured ^{44}Ti activities in emptied glass vials after diffusion treatment A_{vial}, the ^{44}Ti activities in the filtrate after each washing step $A_{step,i}$ and their sum over all washing steps; the ^{44}Ti activities A_{filter} retained on the centrifugation filter used for washing after recovery of nanoparticles for the stock suspension. The mass of the nanoparticles lost in the processing vial m_{vial}, the mass of nanoparticles recovered from there for the washing treatment m_{wash}, the mass nanoparticles m_{filter} lost on the centrifugation filter after washing and the nanoparticle mass recovered after washing m_{rec} as well as the activity of the recovered nanoparticles A_{rec} were calculated using Eqs. (1), (2), (3), (4a, 4b), (5), and (6). (*) denotes washing steps that were performed using 10 mM HCl. The calculated labelling yield and the final fraction of free ^{44}Ti in the suspension after washing are presented. The calculated activity concentration of the nanoparticles, given in Bq/mg, and the mass and activity concentration of the suspension, given in mg/mL and Bq/mL, respectively, were calculated

applied activity of the ^{44}Ti. The ^{44}Ti activity measurements are compiled for the empty processing (glass) vial, for all washing liquids collected after centrifugal filtration and the activity left behind on the filter which could not be recovered for the stock solution after washing. From these activity measurements, the mass of the nanoparticles has been calculated that were retained in the processing vial m_{vial}, the mass that was subjected to the washing treatment $m_{wash} = m_0 - m_{vial}$ and the mass that was retained on the filter after washing m_{filter}, making use of Eqs. (1), (2), (3) and (4a, 4b). Therefore, it is possible to calculate the mass recovered in the stock suspension m_{stock} as well as the activity concentration in the ^{44}Ti-labelled nanoparticles in Bg/mg and of the suspension in Bq/mL. Thus, the table proofs the ease of process control when radiolabelled nanoparticles are used.

The loss of activity in the glass vial used for diffusion treatment can be explained by the retention of nanoparticles adhering to the glass and/or those that could not be recovered by pipetting. The ratio of the activity measured on the emptied glass vial A_{vial} and the applied activity A_0 allows calculating the mass of nanoparticles which could not be recovered from the diffusion treatment vial. The mass which is related to the activity $A_0 - A_{vial}$ is then subjected to the washing treatments by centrifugal filtration using a 10 kDa Amicon® Ultra-15 filter in a 50-mL Falcon vial for 40 min with a relative centrifugal acceleration of 2701 *g* at 4 °C.

The same procedure was applied to label the amorphous silica nanoparticles NM200 (Rasmussen et al. 2013) taken from the JRC Nanoparticle Repository. Centrifugal filtration as described above revealed significant losses of ^{44}Ti in the washing liquids summing up to more than 60%. After 20 washing steps, a fraction of free ^{44}Ti of a little less than 0.01% of the applied ^{44}Ti was revealed in the filtrate. When repeating the centrifugation on 1-mL aliquots of the aqueous stock suspension 4 weeks after radiolabelling, the fraction of free ^{44}Ti in the filtrate was still as low as 0.03% which indicates stable integration of the ^{44}Ti radiolabel in the [^{44}Ti]SiO_2 nanoparticles.

Nanoparticle properties

The DLS and ζ-potential measurements show generally a good agreement between the cold base material and the properties after ^{44}Ti diffusion labelling after applying the same homogenization treatment. The hydrodynamic diameter of the nanoparticles was determined in a 1-mL specimen that was adjusted to a concentration of 0.1 mg/mL immediately after ultrasound homogenization as described in the "Methods" section. Numerical results are presented in Table 3, and intensity vs diameter graphs for ^{44}Ti-labelled and unlabelled nanoparticles are shown in Fig. 1. From Table 3 it can be recognized that the numerical values of the ^{44}Ti-labelled and unlabelled nanoparticles agree satisfactorily.

The ST-01 material is very agglomerated; if real nanosized fractions are needed for experiments, either dispersants should be used during ultrasound homogenization or a size selection has to be performed (Kreyling et al. 2017a, b, c). For SiO_2 NM200 it is difficult to reproduce DLS results for both labelled und unlabelled material as can be seen from the two pairs of curves presented in Fig. 1.

Figure 2 a to d show micrographs from the transmission electron microscopy with the same magnification before and after the diffusion labelling. We applied the GATAN Micrograph software to a series of micrographs for each material to analyse at least 300 nanoparticles. However, especially in the case of the ST-01 material, the highly agglomerated small nanoparticles were frequently not correctly delineated by the software. Therefore, the size measurements were performed manually on all materials in order to apply always the same procedure. The minimum and maximum Feret diameter was determined. The histograms in Fig. 2 visualize the minimum Feret diameter. The quantitative evaluation of the histograms was done by a Gauss fit (in ORIGIN 2019b). In Table 4 the centre x_c of the Gauss fits are compiled ± σ which is determined as the half of the full width at half maximum (FWHM) for the fitted Gauss curve. Additionally, the mean value of the minimum and maximum Feret diameter is reported ± its standard deviation and the aspect ratio of the nanoparticles defined as the maximum Feret diameter divided by the minimum Feret diameter. For each of the nanomaterials, the mean dimension of the nanoparticles before and after diffusion labelling is the same within the error margins; however, slight changes in the range of 1 to 2 nm can be recognized. While the P25 and the NM01004a TiO_2 nanoparticles are slightly bigger after the diffusion labelling, the already small ST-01 nanoparticles appear even smaller after the treatment. Also the SiO_2 nanoparticles appear to be slightly smaller. These findings are consistent whether the results of the Gauss fit on the minimum Feret diameter are concerned or the average size of the nanoparticles is calculated from the

Table 3 Numerical results of dynamic light scattering (DLS) and ζ-potential measurements

Material		Z average in nm	PDI	ζ-pot in mV (*)
TiO2 ST-01	^{44}Ti-labelled	451.3 ± 23.9	0.314 ± 0.028	38.6 ± 1.3
	COLD	412.0 ± 31.9	0.321 ± 0.037	36.4 ± 0.2
TiO2 P25	^{44}Ti-labelled	125.5 ± 1.1	0.178 ± 0.008	24.6 ± 0.8
	COLD	144.9 ± 10.4	0.202 ± 0.070	23.1 ± 0.7
TiO2 NM01004a	^{44}Ti-labelled	127.5 ± 1.5	0.212 ± 0.009	27.3 ± 1.1
	COLD	124.4 ± 3.1	0.206 ± 0.013	35.0 ± 1.1
SiO2 NM200	^{44}Ti-labelled	228.4 ± 11.0	0.359 ± 0.019	− 30.7 ± 0.4
	COLD	243.5 ± 8.5	0.452 ± 0.095	− 30.0 ± 1.4

(*) Measurements at pH ≈ 3 for TiO_2 nanomaterials; at pH ≈ 7 for SiO_2

maximum and minimum Feret diameter. From the aspect ratio, it appears that the NM01004a nanoparticles become slightly more elongated by the treatment

Release of ^{44}Ti radiolabels—leaching experiments

Figure 3 shows the results of the leaching experiments. The three experiments with TiO_2 ST-01 indicate that the nanoparticles are at least stable for 80 days, i.e. the fraction of free ^{44}Ti increases from around $1 \cdot 10^{-5}$ to about $2 \cdot 10^{-4}$ after 80 days (experiments 2 and 3). In experiment 1 a value of $3 \cdot 10^{-3}$ is reached after about 40 days, however, starting from a much higher base value ($5 \cdot 10^{-4}$) since the washing procedure was stopped too early. Nevertheless, this means that even over extended observation periods, nanoparticles in aqueous pH neutral suspensions remain stably ^{44}Ti labelled. The same statement can be made for TiO_2 P25 where

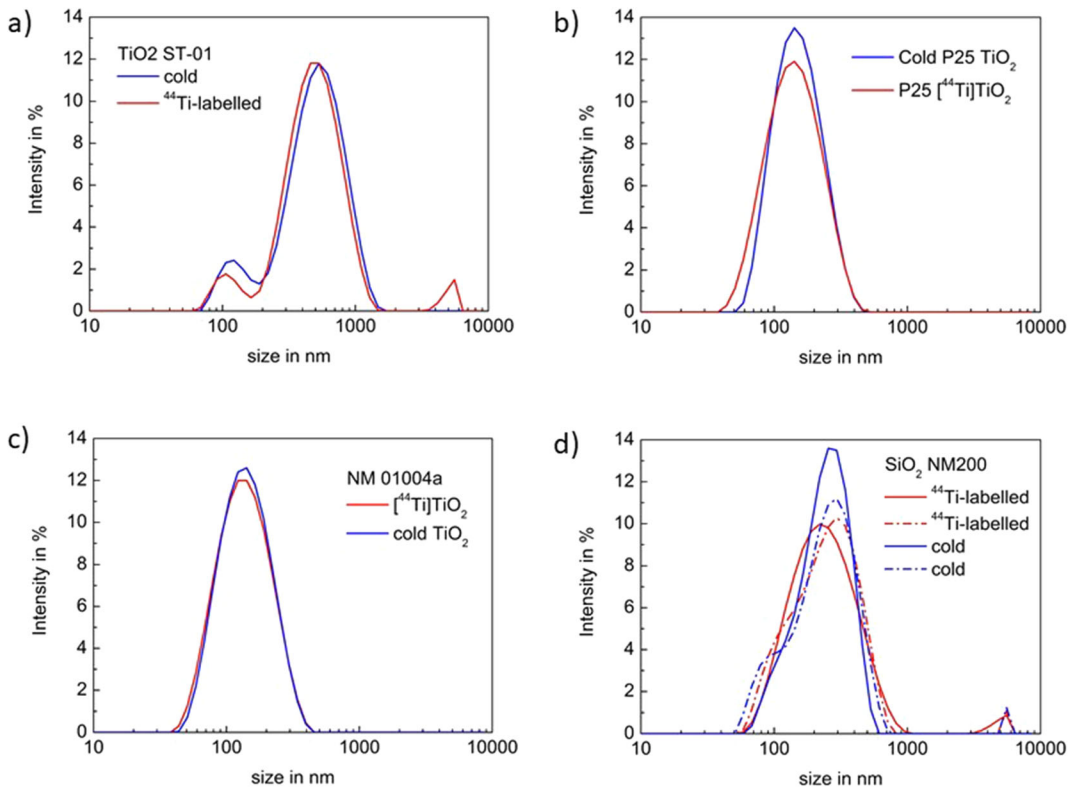

Fig. 1 Comparison of the hydrodynamic diameter of as-received (cold) and ^{44}Ti-labelled nanoparticles of the TiO2 nanomaterials ST-01, P25 and NM01004a and of the SiO2 nanomaterial NM200. As abscissa the intensity of the dynamic light scattering is given

free ^{44}Ti is still in the sub-10^{-3} range after nearly 40 days.

In spite of the different chemical nature of the amorphous SiO_2 matrix, also the NM200 nanoparticles maintain the fraction of free ^{44}Ti in the sub-10^{-3} range up to an observation period of 60 days.

Discussion

The present work was undertaken (i) in order to confirm that different TiO_2 nanomaterials can be diffusion labelled with ^{44}Ti and (ii) that the ^{44}Ti-labelled nanoparticle construct remains stable over several weeks. Moreover, (iii) it was tested whether a chemically different (SiO_2) amorphous material could be stably radiolabelled applying the same non-chemical, purely physical procedure.

The present work is based on the experience gathered by Butz et al. (2011) and by Butz (2012) who investigated various TiO_2 nanomaterials by perturbed angular correlation using ^{44}Ti atoms as nuclear probes. The ^{44}Ti was introduced in the nanomaterials by impregnation of dry powders with ^{44}Ti dissolved in 4 M HCl and subsequent thermal treatment at 180 °C. As described in the "Introduction" section, perturbed angular correlation measurements allow to distinguish whether the radioactive decay of ^{44}Ti takes place on a lattice site in the volume of a nanoparticle or on its surface or close to it. The results of Butz et al. (2011) and of Butz (2012) show unambiguously that impregnation followed by a mild thermal treatment leads to a distribution of the ^{44}Ti atoms in the whole nanoparticles as it can be expected for a diffusive penetration. Since the ^{44}Ti was applied by Butz (2012) in the same chemical form (^{44}Ti dissolved in 4 M HCl) and with a heat treatment at the same temperature of 180 °C for 2 h (here 2.5 h), there is no physical or chemical reason to question the transferability of the results of Butz et al. (2011) and of Butz (2012) to the present case.

The only difference is the about 10 times higher ^{44}Ti activity concentration used by Butz (2012) in order to have sufficient statistics for the γ-γ coincidence measurements. For the present study, we can calculate the number N of used ^{44}Ti atoms from the applied activity A and the physical half-life $T_{½}$ of ^{44}Ti ($N = A \cdot T_{½}/\ln 2$) and get for 65 kBq a number of $1.75 \cdot 10^{14}$ atoms applied on 10 mg of nanoparticles. For nanoparticles with a diameter of 5 nm and of 25 nm, these 10-mg TiO_2 consist of a number of $3.9 \cdot 10^{16}$ and $3.1 \cdot 10^{14}$ nanoparticles, respectively. This implies that only one out of about 200 nanoparticles with a diameter of 5 nm will contain one ^{44}Ti atom. For the larger particles with a diameter of 25 nm, only every second nanoparticle will be labelled with a ^{44}Ti atom. In the present experiments, the activities are on the lower boarder for useful radiotracer experiments, and for biological or toxicological applications, higher activities up to a factor of 1000 could be envisaged. Even in this case, the fraction of radioactive to non-radioactive Ti atoms would still be as low as about $2.5 \cdot 10^{-3}$.

These considerations imply that also for the labelling of SiO_2 nanoparticles, the number of foreign ^{44}Ti atoms is too low to induce modifications of the nanoparticle behaviour. The high ^{44}Ti losses during washing and the consequently low labelling yield experienced with amorphous SiO_2 nanoparticles indicate that the ^{44}Ti atoms are not easily integrated into the amorphous silica structure in spite of the open volume in amorphous structure fostering diffusion. However, the 39% that could not be washed off were stably integrated into the amorphous silica nanoparticle matrix as can be seen from the low leaching visualized in Fig. 3.

In view of the encouraging results with ^{44}Ti diffusion labelling of SiO_2 nanoparticles, this method might also be investigated for the radiolabelling of Al_2O_3 nanoparticles since, as in the case of SiO_2, neutron and charged particle activation of Al_2O_3 does not lead to adequate radionuclides in sufficient quantity for radiotracer studies.

The washing procedure of the nanoparticles was stopped after a washing step in which less than 1 Bq of ^{44}Ti could be detected leaving the number of washing steps to reach this target flexible. This activity limit was chosen in order to have a residual amount of free activity in the range of 10^{-5} as starting point for the leaching experiments. Based on the low leaching experienced with TiO_2 nanoparticles radiolabelled with ^{48}V by direct exposure to a proton beam (Kreyling et al. 2017a, b, c) and in view of intrinsic labelling, which promises best possible integration of the radioactive label in the crystal structure, we expected low leaching rates, which could be difficult to detect on a higher background of residual-free ^{44}Ti activity. Indeed, for all diffusion-labelled nanoparticle types, the fraction of free ^{44}Ti that could be determined in the aqueous suspensions was well below $5 \cdot 10^{-3}$, while the radiolabelling yields for all TiO_2 nanomaterials were high and at least 97.5%. In view of

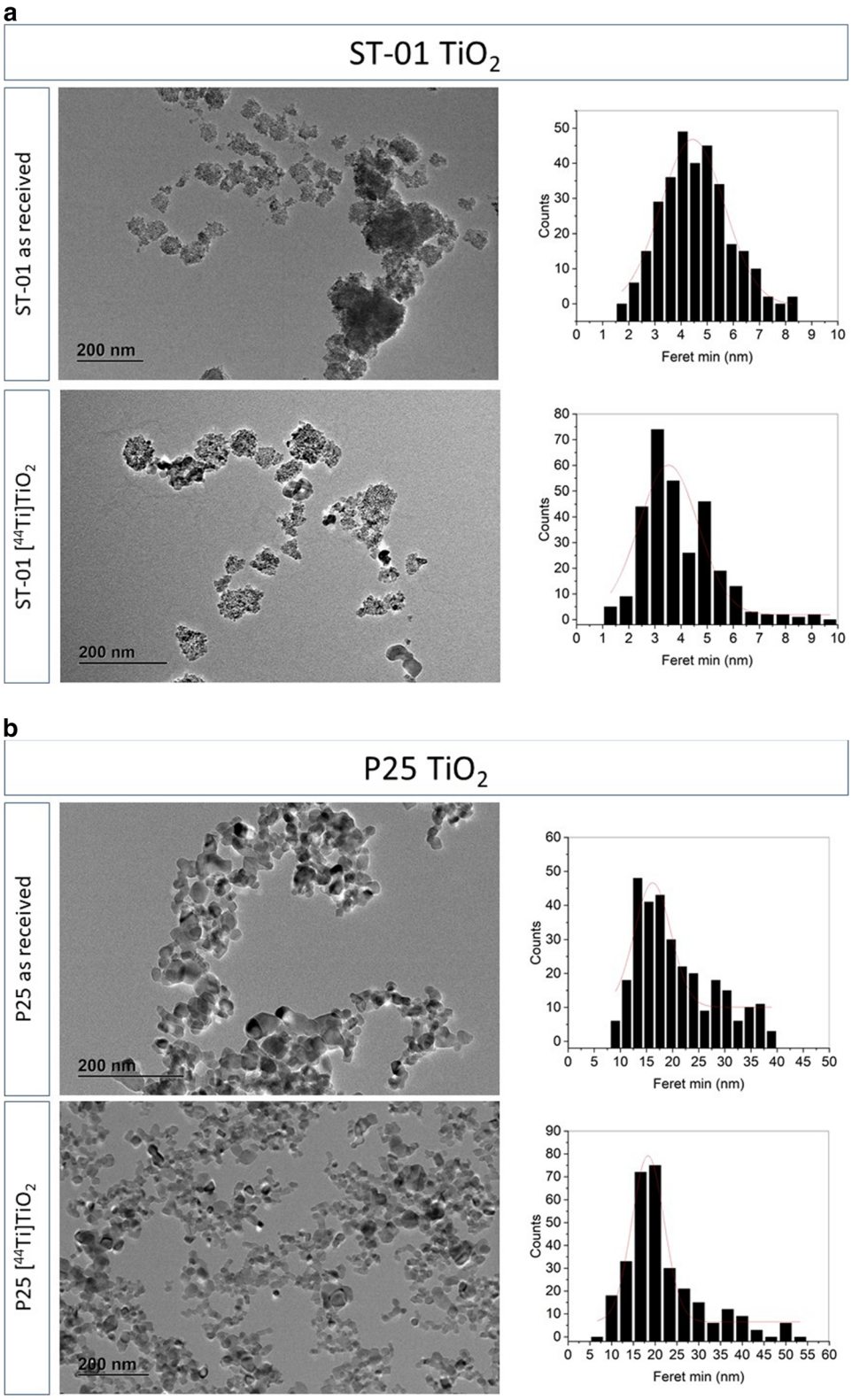
a
ST-01 TiO2
ST-01 as received
200 nm
Counts
Feret min (nm)
ST-01 [44Ti]TiO2
200 nm
Counts
Feret min (nm)
b
P25 TiO2
P25 as received
200 nm
Counts
Feret min (nm)
P25 [44Ti]TiO2
200 nm
Counts
Feret min (nm)

◀ **Fig. 2** **a** TEM micrographs of as-received TiO_2 ST-01 nanoparticles and of diffusion-labelled [^{44}Ti]TiO_2 ST-01 nanoparticles together with the histograms of the minimum Feret diameter of at least 300 nanoparticles. **b** TEM micrographs of as-received P25 TiO_2 nanoparticles and of diffusion-labelled [^{44}Ti]TiO_2 P25 nanoparticles together with the histograms of the minimum Feret diameter of at least 300 nanoparticles. **c** TEM micrographs of NM01004a TiO_2 nanoparticles as received from the JRC Repository of Representative Nanomaterials and [^{44}Ti]TiO_2 NM01004a nanoparticles after diffusion labelling together with the histograms of the minimum Feret diameter of at least 300 nanoparticles. **d** TEM micrographs of NM200 SiO_2 nanoparticles as received from the JRC Repository of Representative Nanomaterials and [^{44}Ti]SiO_2 NM200 nanoparticles after diffusion labelling together with the histograms of the minimum Feret diameter of at least 300 nanoparticles

the differences of these materials as compiled in Table 1, the search for such rather small effects would require sophisticated methods, which were not available in our controlled area. Only TEM specimens got the authorization to leave the controlled area as they exhibit such extremely low levels of radioactivity to overcome radiation protection concerns and concerns to contaminate expensive equipment with long-lived radionuclides.

Especially in the case of intrinsically labelled nanomaterials, the increase of free ^{44}Ti in TiO_2 nanoparticle suspensions over time may also be interpreted as a slow dissolution of the nanoparticles rather than as a phenomena caused by improperly integrated radiolabels. Assuming a homogeneous distribution of the radiolabels in the nanoparticles, the release of about $2{\cdot}10^{-4}$ of the radioactivity after 80 days (in the case of ST-01) would then be equivalent to $2{\cdot}10^{-4}$ of the nanoparticle mass being lost due to dissolution.

However, a possible weakness of the method was that the nanoparticles were impregnated with ^{44}Ti in 4 M HCl, which subjects the nanoparticles to extremely low pH and might modify the nanoparticle surface properties. We may speculate that ^{44}Ti in 4 M HCl is probably a mixture of dissolved Ti hydroxides and chlorohydroxides which are not prone to react with the surface OH groups of the nanoparticles and to bind there. During an increase of the pH, the precipitation of Ti-(OHx)Oy compounds on the nanoparticle surface might occur. However, in view of the proven diffusion of the ^{44}Ti, this would not prevent the ^{44}Ti from penetrating below the nanoparticle surface and becoming distributed in the nanoparticle volume (Butz (2012) and Butz et al. (2011)).

We did not determine the surface hydroxylation of the nanoparticles recovered in aqueous suspension. And we studied the stability only in aqueous suspension at neutral pH. Depending on the envisaged experiments, the chemical nature of the environment the nanoparticles will be subjected to the pH value, and physical parameters such as temperature may be different. Thus, the effects of labelling on essential physicochemical properties and leaching studies have to be performed under the specific experimental conditions for each envisaged application anyway.

Having a look at Table 4 shows that the labelling treatment slightly reduced the size of primary TiO_2 ST-01 and NM200 SiO_2 nanoparticles. In view of the applied processing steps, the most likely explanation is a corrosive attack during the impregnation with ^{44}Ti in 4 M HCl and the following thermal procedure at an elevated temperature of 180 °C. All the following processing steps are much milder and shorter and take place at room temperature. However, the same procedures applied to TiO_2 P25 and NM01004a nanoparticles led to a slight increase of the nanoparticle size which is most likely related to the thermal treatment at 180 °C for 2.5 h.

Whether these slight changes are acceptable must be discussed in the context of the envisaged special application. They are much smaller than the variations reported by Rasmussen et al. (2013, 2014) from TEM measurements performed in different laboratories. However, in the present case, they were performed using the same instrumentation and the same methodology by the same operator. Thus, due consideration should be given to these differences. However, for an envisaged experimental setting, also the agglomeration status of the nanoparticles needs to be considered. The DLS results compiled in Table 3 indicate that in spite of slightly smaller primary ST-01 nanoparticles, the agglomerates might be slightly larger than for the as-received material. For the other nanomaterials, the data show no meaningful difference. A decision needs to weigh these findings against the possible benefit of high detection sensitivity and ease of detection.

The applied temperature of 180 °C for the thermal treatment may become the focus of future improvements of the method. Inagaki et al. (2009) performed isochronous furnace annealing experiments for 1 h in the temperature range between 100 and 800 °C on ST-01 TiO_2 anatase nanoparticles and investigated the annealing effect on the material by XRD and BET measurements.

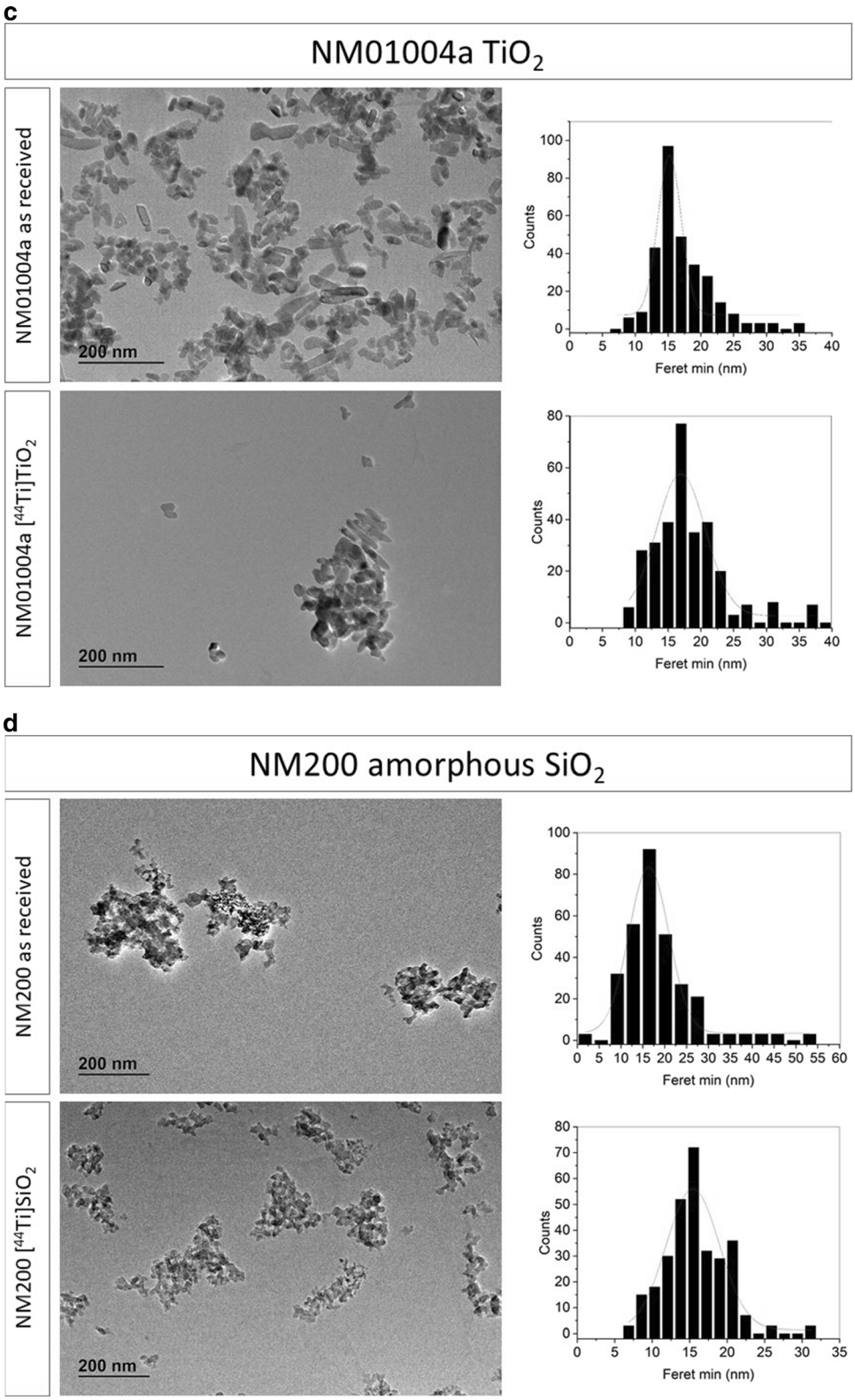

Fig. 2 continued.

Table 4 Results of the quantitative evaluation of TEM micrographs of nanoparticles before and after ^{44}Ti-diffusion labelling

Nanoparticle type	Materials as received				After ^{44}Ti diffusion labelling			
	Feret minimum diameter		Feret diameters		Feret minimum diameter		Feret diameters	
	Average ± SD	$x_c \pm \sigma$	Mean size	Aspect ratio	Average ± SD	$x_c \pm \sigma$	Mean size	Aspect ratio
TiO2 ST-01	4.5 ± 1.2	4.4 ± 1.2	4.8 ± 1.2	1.2 ± 0.4	3.9 ± 1.3	3.5 ± 1.1	4.2 ± 1.2	1.2 ± 0.2
TiO2 P25	20.4 ± 7.3	16.2 ± 3.5	22.8 ± 8.3	1.3 ± 0.2	21.5 ± 8.4	18.4 ± 3.7	23.6 ± 9.2	1.2 ± 0.2
TiO2 NM01004a	16. 9 ± 4.4	15.2 ± 1.8	27.8 ± 8.5	2.3 ± 0.6	17.9 ± 5.4	17.0 ± 3.8	32.8 ± 11.9	2.7 ± 1.1
SiO2 NM200	18.5 ± 7.8	16.4 ± 4.6	19.6 ± 8.0	1.3 ± 0.2	15.6 ± 3.9	15.4 ± 3.5	17.2 ± 4.3	1.2 ± 0.2

The minimum Feret diameter has been evaluated as visualized in the histograms in Fig. 2a to d. The average minimum Feret diameter is presented ± its standard deviation, as well as the centre x_c of the Gauss curve fitted to the histograms ± σ. The mean Feret diameter is reported as calculated from the minimum and maximum Feret diameter ± its standard deviation as well as the aspect ratio (maximum Feret diameter/minimum Feret diameter) ± its standard deviation

The effect of the annealing treatment on the size of single crystalline diffracting anatase domains has been determined from the full width at half maximum (FWHM) of the (101)-diffraction maxima of anatase (Inagaki et al. 2009) making use of Scherrer's formula (cf. Langford and Wilson 1978). The results of Inagaki et al. (2009) showed that the FWHM is constant up to temperatures of about 200 °C and starts to drop from there, indicating growth of the diffracting domains, attributed to a sintering of primary nanoparticles to larger ones of about 20 nm (Inagaki et al. 2009). However, the specific surface area determined by the BET method

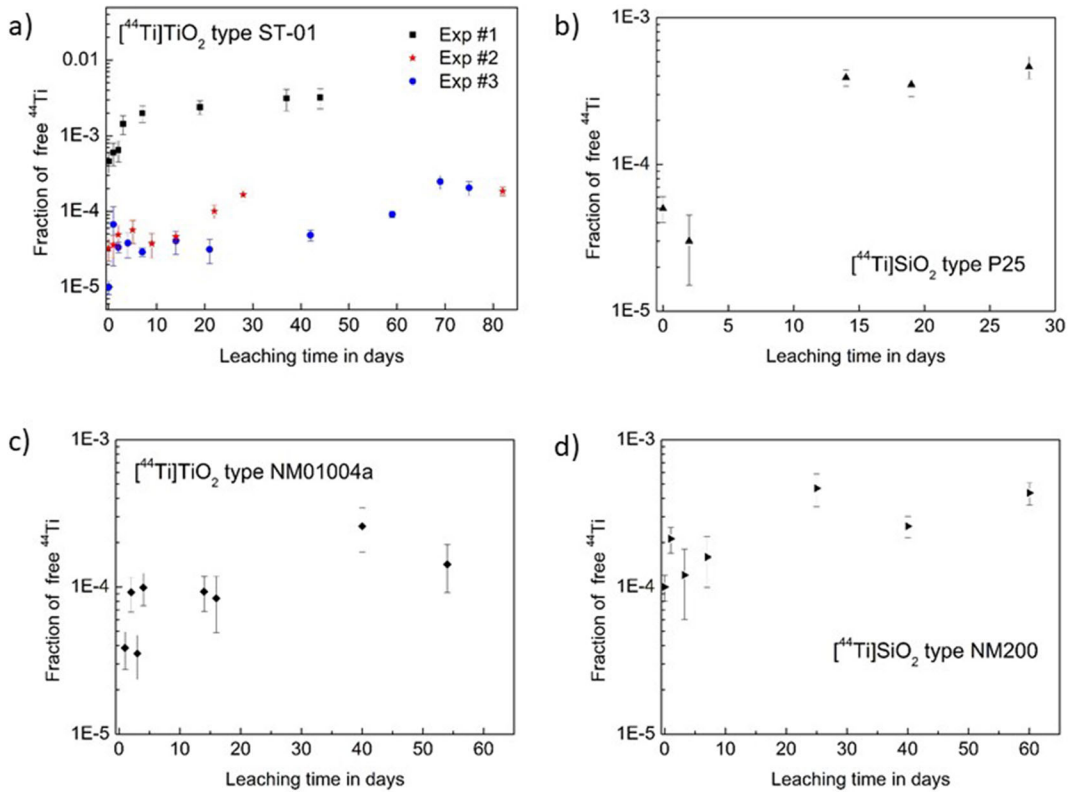

Fig. 3 Leaching experiments—stability of ^{44}Ti-labelled aqueous nanoparticle suspensions. The fraction of free ^{44}Ti determined by γ-spectrometry of the filtrate after centrifugal filtration is presented vs leaching time: for **a** TiO_2 ST-01, **b** TiO_2 P25, **c** TiO_2 NM01004a and **d** SiO_2 NM200

(Brunauer et al. 1938) started to decrease in between the two measurements performed at 100 °C and 200 °C from about 260 m^2g^{-1} to about 210 m^2g^{-1}. Thus, future work might be required to investigate whether slightly lower temperatures (e.g. lower by 10 °C) for the thermal treatment could reduce this loss of surface area without compromising the efficacy of diffusion labelling.

Depending on the ^{44}Ti activity applied in the impregnation treatment and the amount of nanoparticles used, we produced specimens with a specific activity of 1700 Bq/mg (SiO_2) and up to 9200 Bq/mg for TiO_2 ST-01. The minimum detectable activity with our γ-spectrometry equipment is about 0.1 Bq. This implies that about 11 ng ST-01 nanoparticles can be detected. However, on demand this sensitivity can be improved by orders of magnitude. Butz (2012) impregnated 3-mg nanoparticles with 10 μL of ^{44}Ti in 4 M HCl with a specific activity of 20 kBq/μL which translates into 66 kBq/mg. Assuming the same high radiolabelling yield as in the present study, this translates into a detection sensitivity of 1.5 ng of nanoparticles. If we assume to substitute one out of 10,000 Ti atoms by a ^{44}Ti atom, we would obtain nanoparticles with a specific activity of 280 kBq/mg and could push the detection sensitivity down to 0.36 ng of nanoparticles. This appears technically feasible but will require a laboratory with special authorizations for the handling of long-lived open radioactive substances.

Hildebrand et al. (2015) were working with much higher activity concentrations and showed that labelling yields of about 97% could be achieved with ^{45}Ti in P25 TiO_2 nanoparticles that exhibited specific activities of 10 MBq/mg and more. However, due to the much shorter half-live of ^{45}Ti (3.08 h), a much lower number of ^{45}Ti atoms are required to achieve this activity. Pushing the detection sensitivity for ^{44}Ti-labelled nanoparticles further would rather require synthesis of the nanoparticles from ^{44}Ti in a radioactive precursor than labelling. This will no longer be an option to study industrially manufactured nanoparticles.

A further big advantage of radiolabelled nanoparticles is the ease of measurement without special specimen preparation. Outside the scope of the present study which did not use dispersants, pronounced sedimentation occurred in the experiments. This made vortexing mandatory before taking any sample if not immediately after the ultrasound homogenization treatment. Sedimentation is the simplest processing step when performing a size selection (Kreyling et al. 2017a) to ensure experiments being performed with a true nano-fraction of a suspension. However, it may be cumbersome in such cases to determine the mass of nanoparticles in the supernatant. In the present work, we observed for the very agglomerated ST-01 TiO_2 nanoparticles that 1 mL of supernatant after 72 h of sedimentation contained about 90% less ^{44}Ti activity or, in other words, only 10% of the mass per mL than in the vortexed condition. Subjecting the supernatant to a DLS measurement, only one peak appeared and yielded a z-average of 170.1 ± 1.1 nm and a PDI of 0.134 ± 0.007. This illustrates that radiolabelling also offers a simple method to control size selection procedures and to determine the recovered nanoparticle mass in the selected nano-fraction. The same fraction used for the activity measurement can be used for further experimentation without losing material for other analysis techniques to determine the concentration.

Conclusion

Diffusion labelling with commercially available ^{44}Ti is a valuable method for intrinsic radiolabelling of various types of TiO_2 nanoparticles as well as for extrinsic radiolabelling of amorphous silica nanoparticles which offer only very limited possibilities for radiolabelling otherwise. The method is fast and reliable and offers very high detection sensitivity. It requires access to laboratories licenced for handling of long-lived radionuclides but avoids the involvement of nuclear accelerators or reactors. Radiolabelling is stable for periods of several weeks to months in aqueous dispersion at neutral pH. The method may have small effects on the primary particle size with changes in the range of 1 to 2 nm. Whether these may be tolerated must be evaluated on a case-by-case basis depending on the type of application and the benefit gained in detection sensitivity and ease of detection.

Acknowledgements The authors are grateful to Wolfgang W. Kreyling for leaving us the ST-01 material and Karsten Franke and Heike Hildebrand for the P25 material used in the present study, and we thank Douglas Gilliland for discussions on titania and silica chemistry.

Compliance with ethical standards

Conflict of interest The authors declare that they have no conflict of interest.

References

Ahmad L, Bonino G, Cini-Castagnoli G, Fischer SM, Kutschera W, Pau M (1998) Three laboratory measurements of the 44Ti half-life. Phys Rev Lett 80:2550–2553

Bello D, Warheit DB (2017) Biokinetics of engineered nano-TiO2 in rats administered by different exposure routes: implications for human health. Nanotoxicology 11:431–433. https://doi.org/10.1080/17435390.2017.1330436

Brunauer S, Emmett PH, Teller E (1938) Adsorption of gases in multimolecular layers. J Am Chem Soc 60:309–319

Buono S, Burgio N, Hamoudeh M, Fessi H, Hiltbrand E, Maciocco L, Mehier-Humbert S (2007) Brachytherapy: state of the art and possible improvements. Anti Cancer Agents Med Chem 7:411–424. https://doi.org/10.2174/18715200778105864

Butz T, Ryu SB, Jankuhn S, Das SK, Ghoshal (2011) TiO_2 nanomaterials studies by ^{44}Ti(EC)^{44}Sc time differential perturbed angular correlations: volume and surface properties. Defect Diffusion Forum 311:137–158

Butz T (2012) Surface and volume characterization of TiO2 nanomaterials by 44Ti time differential perturbed angular correlation. Radiochim Acta 100:147–153

Chekli L, Brunetti G, Marzouk ER, Maoz-Shen A, Smith E, Naidu R, Shon HK, Lombi E, Donner E (2016) Evaluating the mobility of polymer-stabilised zero-valent iron nanoparticles and their potential to co-transport contaminants in intact soil cores. Environ Pollut 216:636e645

Chu SYF, Ekström LP, Firestone RB (1999) The Lund/LBNL Nuclear Data Search, Version 2.0, February 1999; WWW Table of Radioactive Isotopes. http://nucleardata.nuclear.lu.se/toi/nuclide.asp?iZA=220044

Cotogno G, Simonelli F, Holzwarth U, Gibson N (2016) In: Llop Roig J, Gómez-Vallejo V, Gibson N (eds) Neutron activation of nanoparticles. In: isotopes in nanoparticles: fundamentals and applications. Pan Stanford publishing Pte. Ltd, pp 315–333

Coutris C, Joner EJ, Oughton DH (2012) Aging and soil organic matter content affect the fate of silver nanoparticles in soil. Sci Total Environ 420:327–333. https://doi.org/10.1016/j.scitotenv.2012.01.027

Dieci MB, Liu M, Dinh QT, Nguyen J (2017) Precision engineering of targeted nanocarriers WIREs. Nanomed Nanobiotechnol 10:e1511. https://doi.org/10.1002/wnan.1511

EFSA (2018) European food safety agency, panel on food additives and nutrient sources added to food (ANS), Younes M, Aggett P, Aguilar F, Crebelli R, Dusemund B, Filipi M, Frutos MJ, Galtier P, Gott D, Gundert-Remy U, Kuhnle GG, Leblanc JC, Lillegaard IT, Moldeus P, Alicja A, Oskarsson A, Stankovic I, Waalkens-Berendsen I, Woutersen RA, Wright M, Boon P, Chrysafidis D, Gürtler R, Mosesso P, Parent-Massin D, Tobback P, Kovalkovicova N, Rincon AM, Tard A, Lambré C (2018) Re-evaluation of silicon dioxide (E 551) as a food additive. EFSA Journal 16(1):5088. https://doi.org/10.2903/j.efsa.2018.5088

Gesenhues U (1997) Doping of TiO_2 pigments by Al^{3+}. Solid State Ionics 101-103:1171–1180

Gibson N, Holzwarth U, Abbas K, Simonelli F, Kozempel J, Cydzik I, Cotogno G, Bulgheroni A, Gilliland D, Ponti J, Franchini F, Marmorato P, Stamm H, Kreyling W, Wenk A, Semmler-Behnke BS, Maciocco L, Burgio N (2011) Radiolabelling of engineered nanoparticles for in vitro and in vivo tracing applications using cyclotron accelerators. Arch Toxicol 85:751–773

Goel S, Chen F, Ehlerding EB, Cai W (2014) Intrinsically radiolabeled nanoparticles: an emerging paradigm. Small 10(19):3825–3830. https://doi.org/10.1002/smll.201401048

Häfeli UO, Roberts WK, Pauer GJ, Kraeft S-K, Macklis RM (2001) Stability of biodegradable rhenium (re-186 and re-188) microspheres after neutron activation. Appl Radiat Isot 54:869–879

Hamoudeh M, Fessi H, Mehier H, Al Faraj A, Canet-Soulas E (2008) Dirhenium decacarbonyl-loaded PLLA nanoparticles: influence of neutron irradiation and preliminary in vivo administration by the TMT technique. Int J Pharm 348:125–136

Hamoudeh M, Salim H, Barbos D, Paunoiu C, Fessi H (2007) Preparation and characterization of radioactive dirhenium decacarbonyl-loaded PLLA nanoparticles for radionuclide intra-tumoral therapy. Eur J Pharm Biopharm 67:597–611

Hildebrand H, Franke K (2012) A new radiolabeling method for commercial Ag0 nanopowder with 110mAg for sensitive nanoparticle detection in complex media. J Nanopart Res 14:#1142

Hildebrand H, Schymura S, Holzwarth U, Gibson N, Dalmiglio M, Franke K (2015) Strategies for radiolabelling of commercial TiO2 nanopowder as a tool for sensitive nanoparticle detection in complex matrices. J Nanopart Res 17:#278. https://doi.org/10.1007/s11051-015-3080-8

Holzwarth U, Bellido E, Dalmiglio M, Kozempel J, Cotogno G, Gibson N (2014) ^{7}Be-recoil radiolabelling of industrially manufactured silica nanoparticles. J Nanopart Res 16:2574. https://doi.org/10.1007/s11051-014-2574-0

Holzwarth U, Bulgheroni A, Gibson N, Kozempel J, Cotogno G, Abbas K, Simonelli F, Cydzik I (2012) Radiolabelling of nanoparticles by proton irradiation: temperature control in nanoparticulate powder targets. J Nanopart Res 16:880. https://doi.org/10.1007/s11051-012-0880-y

Horikoshi S, Minatodani Y, Sakai H, Abe M, Serpone N (2011) Characteristics of microwaves on second generation nitrogen-doped TiO2 nanoparticles and their effect on photoassisted processes. J Photochem Photobiol A 217:191–200

Inagaki M, Kondo N, Nonaka R, Ito E, Toyoda M, Sogabe K, Tsumura T (2009) Structure and photoactivity of titania derived from nanotubes and nanofibres. J Hazard Mater 161:1514–1152

Jiang Q, Zhang SH, Li JC (2004) Grain-size dependent diffusion activation energy in nanomaterials. Solid State Commun 130: 581–584

Jin Y, Tan Z, Hu L, Yu S, Liu J, Jiang G (2017) Isotope tracers to study the environmental fata and bioaccumulation of metal-containing engineered nanoparticles: techniques and applications. Chem Rev 117:4462–4487. https://doi.org/10.1021/acs.chemrev.6b00693

Kleiven M, Rosseland BO, Teien HC, Joner EJ, Oughton DH (2018) Route of exposure has a major impact on uptake of silver nanoparticles in Atlantic Salmon (Salmo salar). Environ Toxicol Chem 37:2895–2903

Kreyling WG, Holzwarth U, Haberl N, Kozempel J, Hirn S, Wenk A, Schleh C, Schäffler M, Lipka J, Semmler-Behnke M, Gibson N (2017a) Quantitative biokinetics of titanium dioxide nanoparticles after intravenous injection in rats: part 1. Nanotoxicology 11:434–442

Kreyling WG, Holzwarth U, Schleh C, Kozempel J, Wenk A, Haberl N, Hirn S, Schäffler M, Lipka J, Semmler-Behnke M, Gibson N (2017b) Quantitative biokinetics of titanium dioxide nanoparticles after oral application in rats: part 2. Nanotoxicology 11:443–453

Kreyling WG, Holzwarth U, Haberl N, Kozempel J, Wenk A, Hirn S, Schleh C, Schäffler M, Lipka J, Semmler-Behnke M, Gibson N (2017c) Quantitative biokinetics of titanium dioxide nanoparticles after intratracheal instillation in rats: part 1. Nanotoxicology 11:454–464

Krug HF (2014) Nanosafety research – are we on the right track? Angew Cem Int Ed 53:2–18

Kunz-Schughart LA, Dubrovska A, Peitzsch C, Ewe A, Aigner A, Schellenburg S, Muders MH, Hampel S, Cirillo G, Iemma F, Tietze R, Alexiou C, Stephan H, Zarschler K, Vittorio O, Kavallaris M, Parak WJ, Mädler L, Pokhrel S (2017) Nanoparticles for radiooncology: Mission, vision, challenges. Biomaterials 120:155–184. https://doi.org/10.1016/j.biomaterials.2016.12.010

Langford JI, Wilson AJC (1978) Scherrer after sixty years: a survey and some new results in the determination of crystallite size. J Appl Crystallogr 11:102–113. https://doi.org/10.1107/S0021889878012844

Llop J, Gòmez-Vallejo V, Gibson N (2013) Quantitative determination of the biodistribution of nanoparticles: could radiolabelling be the answer? Nanomedicine 8:1035–1038

Marmorato P, Simonelli F, Abbas K, Kozempel J, Holzwarth U, Franchini F, Ponti J, Gibson N, Rossi F (2011) 56Co-labelled radioactive Fe3O4 nanoparticles for in vitro uptake studies on Balb/3T3 and Caco-2 cell lines. J Nanopart Res 13:6707–6716. https://doi.org/10.1007/s11051-011-0577-7

OECD (2015) Dossier on titanium dioxide-part 1/1 - NM 105; series on the safety of manufactured NanomaterialsNo. 54 http://www.oecd.org/officialdocuments/publicdisplaydocumentpdf/?cote=env/jm/mono(2015)17/part1/1&doclanguage=en

Oughton DH, Hertel-Aas T, Pellicer E, Mendoza E, Joner ER (2008) Neutron activation of engineered nanoparticles as a tool for tracing their environmental fate and uptake in organisms. Environ Toxicol Chem 9:1883–1887

Pérez-Campaña C, Gómez-Vallejo V, Martin A, San Sebastián E, Moya SE, Reese T, Ziolo RF, Llop J (2012) Tracing nanoparticles in vivo: a new general synthesis of positron emitting metal oxide nanoparticles by proton beam activation. Analyst 137:4902–4906

Pérez-Campaña C, Gómez-Vallejo V, Puigivila M, Martín A, Calvo-Fernández T, Moya SE, Ziolo RF, Reese T, Llop J (2013) Biodistribution of different sized nanoparticles assessed by positron emission tomography: a general strategy for direct activation of metal oxide particles. ACS Nano 7: 3498–3505

Ponti J, Colognato R, Franchini F, Gioria S, Simonelli F, Abbas K, Uboldi C, Kirkpatrick CJ, Holzwarth U, Rossi F (2009) A quantitative in vitro approach to study the intracellular fate of gold nanoparticles: from synthesis to cytotoxicity. Nanotoxicology 3:296–306. https://doi.org/10.1080/17435390903056384

Pruszyński M, Loktionova NS, Filosofov DV, Rösch F (2010) Post-elution processing of 44Ti/44Sc generator-derived 44Sc for clinical application. Appl Radiat Isot 68:1636–1641

Radchenko V, Engle JW, Medvedev DG, Maassen JM, Naranjo CM, Unc GA, Meyer CAL, Mastren T, Brugh M, Mausner L, Cutler CS, Birnbaum ER, John KD, Nortier FM, Fassbender ME (2017) Proton-induced production and radiochemical isolation of 44Ti from scandium metal targets for 44Ti/44Sc generator development. Nucl Med Biol 50:25–32. https://doi.org/10.2106/j.nucmedbio.2017.03.006

Rasmussen K, Mast J, De Temmerman PJ, Verleysen E, Waegeneers N, Van Steen F, Pizzolon JC, De Temmerman L, Van Doren E, Jensen KA et al. (2014) JRC science and policy reports. Titanium dioxide, NM-100, NM-101, NM-102, NM-103, NM-104, NM-105: characterization and physicochemical properties. JRC repository: NM-series of representative manufactured Nanomaterials. European Commission, Joint Research Centre, Institute for Health and Consumer Protection, 2014, EUR 26637 EN

Rasmussen K, Mech A, Mast J, De Temmerman PJ, Waegeneers N, Van Steen F, Pizzolon J-C, De Temmerman L, Van Doren E, Jensen KA, et al. (2013) Synthetic amorphous silicon dioxide (NM-200, NM-201, NM-202, NM-203, NM-204): characterisation and physico-chemical properties. JRC repository: NM-series of representative manufactured nanomaterials. European Commission, Joint Research Centre, Institute for Health and Consumer Protection, 2013, EUR 26046 EN

Scheinberg DA, Grimm J, Heller DA, Stater EP, Bradbury M, McDevitt MR (2017) Advances in the clinical translation of nanotechnology. Curr Opin Biotechnol 46:66–73. https://doi.org/10.1016/j.copbio.2017.01.002

Schleh C, Holzwarth U, Hirn S, Wenk A, Simonelli F, Schäffler M, Möller W, Gibson N, Kreyling WG (2013) Biodistribution of inhaled gold nanoparticles in mice and the influence of surfactant protein D. J Aerosol Med Pulm Drug Deliv 26:24–30. https://doi.org/10.1089/jamp.2011.0951

Shibata T, Bunker BA, Zhang Z, Meisel D, Vardeman CF, Gezelter JD (2002) Size-dependent spontaneous alloying of Au-Ag nanoparticles. J Am Chem Soc 124:11989–11996

Simonelli F, Marmorato P, Abbas K, Ponti J, Kozempel J, Holzwarth U, Franchini F, Rossi F (2011) Cyclotron production of radioactive CeO2 nanoparticles and their application

for in-vitro uptake studies. IEEE Trans Nanobiosci 10:44–50. https://doi.org/10.1109/TNB.2011.2119491

Taurozzi JS, Hackley VA, Wiesner MR (2011) Ultrasonic dispersion of nanoparticles for environmental, health and safety assessment – issues and recommendations. Nanotoxicology 5:711–729. https://doi.org/10.3109/17435390.2010.528846

Totaro S, Cotogno G, Rasmussen K, Pianella F, Roncaglia M, Olsson H, Riego Sintes JM, Crutzen HP (2016) The JRC Nanomaterials repository: a unique facility providing representative test materials for nanoEHS research. Regul Toxicol Pharmacol 81:334–340

Vandebriel RJ, Vermeulen JP, van Engelen LB, de Jong B, Verhagen LM, de la Fonteyne-Blankestijn HME, de Jong WH (2018) The crystal structure of titanium dioxide nanoparticles influences immune activity in vitro and in vivo. Particle Fibre Toxicol 15:#9. https://doi.org/10.1186/s12989-018-0245-5

Vitorge E, Szenknect S, Martins JMF, Barthès V, Gaudet JP (2014) Comparison of three labeled silica nanoparticles used as tracers in transport experiments in porous media. Part II: transport experiments and modeling. Environ Pollut 184: 613e619. https://doi.org/10.1016/j.envpol.2013.08.016

Vollath D (2008) Nanomaterials –an introduction to synthesis, Properties and Applications. Wiley-VCH Verlag GmbH & Co. KGaA, Weinheim

Weiss C, Diabate S (2011) A special issue on nanotoxicology. Arch Toxicol 85:705–706

Xie G, Sun J, Zhong G, Shi L, Zhang D (2010) Biodistribution and toxicity of intravenously administered silica nanoparticles in mice. Arch Toxicol 84:183–190. https://doi.org/10.1007/s00204-009-0488-x

Zhang ZY, Zhao YL, Chai ZF (2009) Applications of radiotracer techniques for the pharmacology and toxicology studies of nanomaterials. Chin Sci Bull 54:173–182